MATERIALS ENGINEERING

Direct 4D printing via active composite materials

Zhen Ding,[1]* Chao Yuan,[2,3]* Xirui Peng,[4] Tiejun Wang,[3] H. Jerry Qi,[2†] Martin L. Dunn[1†]

We describe an approach to print composite polymers in high-resolution three-dimensional (3D) architectures that can be rapidly transformed to a new permanent configuration directly by heating. The permanent shape of a component results from the programmed time evolution of the printed shape upon heating via the design of the architecture and process parameters of a composite consisting of a glassy shape memory polymer and an elastomer that is programmed with a built-in compressive strain during photopolymerization. Upon heating, the shape memory polymer softens, releases the constraint on the strained elastomer, and allows the object to transform into a new permanent shape, which can then be reprogrammed into multiple subsequent shapes. Our key advance, the markedly simplified creation of high-resolution complex 3D reprogrammable structures, promises to enable myriad applications across domains, including medical technology, aerospace, and consumer products, and even suggests a new paradigm in product design, where components are simultaneously designed to inhabit multiple configurations during service.

INTRODUCTION

Four-dimensional (4D) printing is a term that was recently coined (*1*) to describe the integration of 3D printing and active material technologies to realize printed components that can be switched between multiple configurations via an environmental stimulus, for example, heat or moisture (*2*–*16*). To date, hydrogels (*17*–*19*) and shape memory polymers (SMPs) (*20*–*26*) are the two main active polymers used in 4D printing. In hydrogel-based 4D printing, hydrogels are integrated with a nonswelling polymer or filament. When the printed structure is immersed in a solvent, the hydrogel swells, creating mismatch strains between the two materials that lead to overall shape change (*4*, *11*, *12*). The advantage of this approach is that it does not require programming after printing; however, there are a few drawbacks. First, hydrogels are soft, and thus, the stiffness of the printed structure is relatively low. This can be overcome by a composite strategy, where the soft gel is combined with a stiff SMP (*11*, *12*). Second, the swelling mechanism is based on species transport (diffusion), and thus, the responsive speed is relatively slow, especially for large structures. For example, although the active element (a hinge) in Tibbits' work is small (~0.8 mm), it takes about 7 min to achieve a bending angle of 36° (*4*). Third, the actuated shape by swelling is not stable, because it will change with the subsequent loss of solvent in the hydrogel if the environmental condition is changed. Photocured SMPs have been used in 4D printing with both commercial and research printing technologies based on photopolymer inkjetting (*2*, *10*, *27*) and projection microstereolithography (*14*, *16*). 4D printing with SMPs generally requires a series of steps (Fig. 1A): (i) synthesis/processing by 3D printing; thermomechanical programming, including (ii) heating, (iii) mechanical loading, (iv) cooling, and (v) removal of load; and (vi) deployment/actuation. Thermomechanical programming often requires special jigs and fixtures to apply mechanical loads and a well-controlled thermal environment (*22*). However, 4D printing with SMPs also offers the advantages of a relatively stiff structure and relatively high actuation speed; both are orders of magnitude higher than those obtained with printed hydrogels. As a result, an attractive approach in improving SMP-based 4D printing has been to simplify the mechanical loading to uniaxial and to combine it with geometric complexity that is easily achievable by 3D printing to enable programmed 3D configurations (*2*, *3*, *10*, *28*). It should be noted that, very recently, digital photopolymerization was used to simplify the shape-changing process of thin films via gel swelling/wax uptake (*29*) or desolvation (*30*). However, these methods are limited to single-layer printing and require the intake of other materials.

We propose a new direct 4D printing approach with SMPs, where we integrate the programming steps into the 3D printing process. The sample in our method is ready for shape changing just after printing without any composition change required by gel-based 4D printing or the thermomechanical training required by SMP-based 4D printing. As a result, the 3D-printed component can directly change its shape rapidly upon heating (Fig. 1B). To do this, we effectively control the photopolymerization process during printing to enable 3D components with complex geometric form at high spatial resolution in a way that, when removed from the build tray, they exhibit high-fidelity features but with controlled built-in strains. The deployment step then simply involves heating the component upon which the shape transformation occurs at a time scale controlled by the heat transfer. This second stable shape largely remains stable in later variations in temperature, such as cooling back to room temperature and heating again. By exploiting the shape memory effect of the glassy polymer, a third shape, or even multiple shapes, can be programmed by thermomechanical loading, and the material will always recover back to the permanent (second) stable shape upon heating. As a result, the transformation between two well-defined shapes is simple and direct, and can be done with complex geometrical components with high fidelity. Unlike the previous 4D printing where the programmed shape is temporary and the printed shape is permanent, our new direct 4D printing results in the printed shape being temporary and the second shape, evolved with time under environmental stimuli, being permanent; the 4D-printed shape is relatively stiff at room temperature.

To enable design with our new 4D printing process, we created a theoretical model that incorporates the key elements, including the material behaviors during the processing/programming and deployment phases and 3D printing processing parameters. We implemented the model into a finite element code, used it to simulate the 4D printing, and found good agreement with experiments using components that we

[1]SUTD Digital Manufacturing and Design Centre, Singapore University of Technology and Design, Singapore 487372, Singapore. [2]The George Woodruff School of Mechanical Engineering, Georgia Institute of Technology, Atlanta, GA 30332, USA. [3]State Key Laboratory for Strength and Vibration of Mechanical Structures, School of Aerospace Engineering, Xi'an Jiaotong University, Xi'an 710049, China. [4]School of Mechanical Engineering, Zhejiang University, Hangzhou 310027, China.
*These authors contributed equally to this work.
†Corresponding author. Email: qih@me.gatech.edu (H.J.Q.); martin_dunn@sutd.edu.sg (M.L.D.)

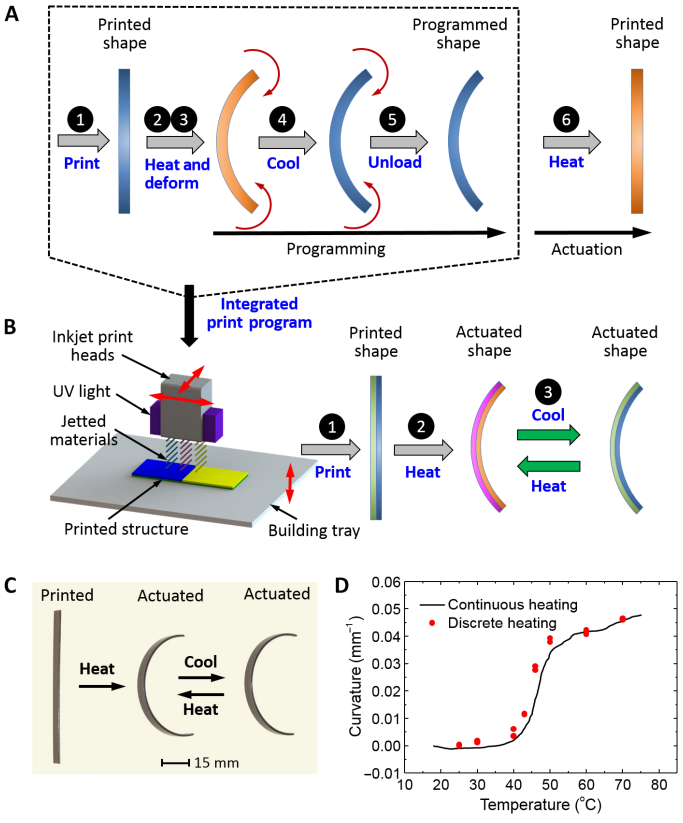

Fig. 1. The concept of direct 4D printing and its experimental demonstration. (**A**) Previous SMP-based 4D printing requires five steps to achieve the programmed shape. (**B**) The direct 4D printing approach exploits the ability to print controlled multimaterial composites to integrate the five steps into a single one. (**C**) Experimental demonstration of two-layer strips (80 mm × 5 mm × 0.6 mm, with each layer 0.3 mm) that have been designed and fabricated to be printed as a flat strip (the temporary shape) and then, when heated, transform into a curved shape (the permanent shape) that remains largely unchanged upon further cooling and heating. (**D**) Measured curvature of the bilayer as a function of temperature during heating to deploy the bilayer from its flat to the curved shape. Both continuous and discrete heating achieve the same curvatures: The former are heated from 18°C at a rate of 2°C/min, whereas the latter are immersed in water for 20 s at a prescribed temperature.

designed, fabricated, and tested. This implementation demonstrates the capabilities of the new approach and the key parameters involved.

RESULTS

Our direct 4D printing approach is illustrated in Fig. 1, where it is compared with existing approaches of 4D printing using SMPs. It integrates five separate printing and programming steps (Fig. 1A) into a single one, resulting in great simplicity. After printing a component in a temporary configuration at high resolution (with the polyJet process that jets ink droplets of multimaterial materials in a layer, smooths them, and cures them with ultraviolet light, we routinely achieve features with a resolution of about 50 μm in plane and 15 μm through the thickness), it can simply be heated to transform it into its second permanent configuration (Fig. 1B). Here, a laminated strip is printed with two materials—an SMP and an elastomer. At room temperature, the SMP is glassy with a modulus of ~1 GPa, which is two to three orders of magnitude stiffer than the elastomer (E ~ 1 MPa); see the Supplementary Materials for details regarding thermomechanical properties of the materials. In the printed (temporary) configuration, the stiff SMP provides mechanical rigidity, and the specific behaviors can be designed with the help of computational simulations (see Materials and Methods and the Supplementary Materials). The as-printed elastomer contains a compressive biaxial stress that can be controlled by the material composition and printing process parameters, for example, temperature, light intensity, photocuring time, and layer printing time. Strong bonding of the elastomer to the SMP builds the compressive strain into the composite while maintaining stability at room temperature and high fidelity in the geometrical resolution, as determined by its design in a 3D computer-aided design (CAD) file. After it is removed from the build tray, the laminate can be deployed into a new (permanent) shape by heating, as shown by the experimental demonstration in Fig. 1C, where the permanent shape is a curved laminate.

Figure 1D shows the curvature evolution during deployment of printed laminates. As the temperature is raised, the coefficient of thermal expansion (CTE) mismatch between the SMP (in glassy state) and the elastomer (in rubbery state) tends to drive the laminate to bend. As the temperature approaches T_g of the SMP, the SMP softens and relaxes the constraint on the built-in compressive strains in the elastomer, effectively releasing them. When combined with the CTE mismatch between the SMP and the elastomer, this results in deformation of the component as mechanical equilibrium is established. The bending rate is most pronounced as the glass transition of the SMP is approached (~45°C), and it saturates at about 60°C, reaching a maximum. As the temperature increases above T_g, the SMP modulus is comparable to that of the elastomer, consistent with standard rubber elasticity. The CTEs of the two materials are also comparable above T_g, and this contributes to the existence of a plateau in the curvature evolutions (see the thermal strains in fig. S1C). Figure 1D also shows results obtained in two ways: (i) continuous heating, where the sample is put in water at 18°C and the sample curvature is measured as the water temperature is raised at a rate of 2°C/min, and (ii) discrete measurements, where samples are immersed in water that has been held at a prescribed temperature and measured 20 s after immersion. Results for both are consistent, which illustrates that, during deployment, viscous effects of the SMPs are not significant, nor is diffusion of moisture into the polymer during immersion in water. When the laminate is cooled back to room temperature after deployment, CTE mismatch between the materials can lead to further deformation, but this is modest because the CTEs of the two materials are similar above T_g. Whereas the CTE mismatch increases as the temperature decreases below T_g, the SMP stiffness concurrently increases significantly (fig. S1A), serving to lock the laminate into the bent shape. Therefore, as shown in Fig. 1C, the component is basically "locked" or "reshaped" into the permanent shape, achieved by simply heating the printed component to the elevated temperature. We show later that from this permanent shape, a component can be heated, reformed into a new shape, and then cooled to fix it in another (temporary) shape by exploiting the shape-fixing ability of the SMP. Reheating returns the sample to the permanent shape (not the printed shape), and this process can be repeated many times.

Figure 2 shows results from systematic studies to understand the mechanisms of shape change and elucidate the role of key design parameters. We tailor the built-in compressive strain in the elastomer by controlling the printing time of each layer. Figure 2A shows measured compressive strains versus layer printing time obtained from experiments, where we print a layer of elastomer and then measure the expansion that results from the built-in stresses when we remove it from the

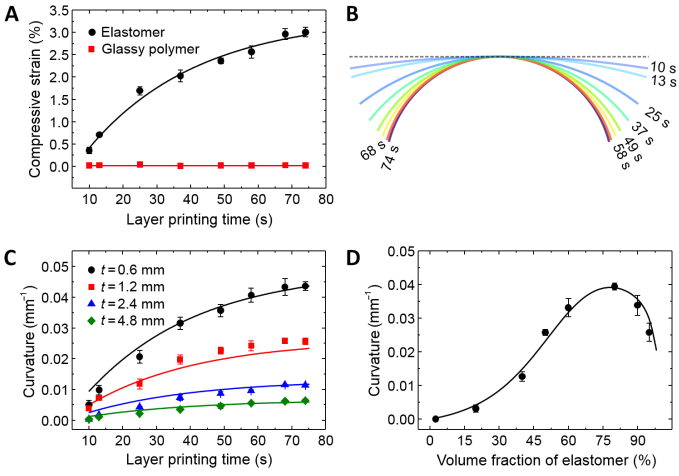

Fig. 2. Basic understanding of the parameters involved in direct 4D printing. (**A**) Measured (symbols) and fitted (curves) compressive strain built into each material (strips of dimensions 60 mm × 8 mm × 1.2 mm) as a function of the printing time for each layer. (**B**) Measured permanent shape of printed flat bilayer samples (60 mm × 6 mm × 0.6 mm, with each layer having equal thickness) as a function of layer printing time. (**C**) Measured (symbols) and simulated (curves) curvature of bilayers (60 mm × 5 mm × *t* mm) with elastomer and SMP layers of equal thickness as a function of total layer thickness (*t*) and layer printing time. (**D**) Measured (symbols) and simulated (curves) curvature of bilayers (60 mm × 5 mm × 1.2 mm) as a function of volume (thickness) fraction of elastomer. The curvatures in (B) to (D) were measured after the samples were heated to 62°C and held for 20 s.

build tray. By varying the layer print time over a range from 10 to 74 s, we can tailor the built-in strain by over an order of magnitude. Fundamentally, this arises from the details of the photochemical reaction kinetics during the layer-by-layer curing process. More detailed fundamental studies would be necessary to fully understand the underlying mechanisms. Instead, here, we characterize it with a simple empirical model. We have found that the compressive strain is roughly equibiaxial, although there is some variation with orientation in the build tray (for example, 3.1% along the *x* axis versus 3.6% along the *y* axis for a layer printing time of 74 s). We ignore the anisotropy here, but it would be straightforward to consider it in a more detailed study. Dynamic mechanical analysis (DMA) tests show that the glass transition temperatures of the SMP and elastomer are 62°C and 8°C, respectively. We note that the printing time has little influence on both the storage modulus and glass transition temperature of either material (fig. S1, A and B).

Figure 2B shows a series of laminate strips (60 mm × 5 mm × 0.6 mm, with each material layer 0.3 mm) that were printed as flat strips with various printing times between each print layer. Note that the printing process proceeds by printing 30-μm-thick layers until the thickness of 0.3 mm is achieved. Samples were then removed from the build tray and heated to deploy them into their permanent shapes. The curvature of the permanent shape results from the built-in compressive strain in Fig. 2A and can be controlled via the printing time. Figure 2C shows quantitative results for the curvature developed as a function of printing time for a series of bilayers with elastomer and SMP layers of equal thickness but with a total thickness that spans a range of nearly an order of magnitude (0.6 to 4.8 mm). The thickness and printing time combine to allow curvature variations of well over an order of magnitude. Also shown in Fig. 2C are results from simulations done with a model that accounts for the temperature-dependent thermomechanical behavior of each material and the experimentally determined built-in compressive strain in the elastomer from Fig. 2A (see the Supplementary Materials for details of the model and its implementation into a finite element code). The simulations describe the observed behavior well and provide confidence that the behavior can be exploited in broader geometrical configurations (the power of the 3D printing approach) to create sophisticated components and that the model can be used to design the appropriate geometrical and processing parameters. The simulations also help reveal the shape change mechanism, qualitatively and quantitatively. Figure 2D shows the results of both experiments and simulations on the effect of the SMP to elastomer thickness ratio on the curvature for a series of laminates expressed in terms of the elastomer volume fraction. Measurements and simulations are in reasonable agreement; they also demonstrate that there is an optimal geometrical configuration that can be designed to maximize the deformation after deployment. It should be noted that shape alternation due to volume change in active polymer was reported before. For example, Xie and Xiao (*31*) reported that curing induced shrinkage and some CTE mismatch immediately after fabrication (that is, after demolding and cooling from the curing temperature) to induce shape change, although it was unclear which one was the major contributor. In our work, the shape change only occurs when we stimulate the sample by heating, and the shape would not change back upon cooling. By using our theoretical model, we can quantify the ratio between the built-in compressive strain and CTE mismatch strain toward bending, as shown in fig. S2. It can be seen that the dominant contribution to the shape change is from the built-in compressive strain. The contribution to overall curvature from CTE is ~38% when the layer printing time is 10 s, whereas it declines to only ~8% when the layer printing time is 72 s.

Figures 3 and 4 show the application of the ideas of direct 4D printing to structural elements in an attempt to convey the flexibility that is offered through the combination of geometrical, material, and processing design parameters. In all examples, the basic idea is to print samples in flat layered configurations that are simple to design and economical to print in terms of both printing time and material wastage because no support material is needed. Then, by the simple heating step, they are deployed to realize various 3D permanent shapes. Although not studied here, samples can also be designed to create various modes of actuation and specific actuation forces, or designed to exhibit desired structural stiffness in the final configuration. Each of the examples in Fig. 3 uses bending between the elastomer and SMP to drive the deformation, but the geometrical configuration of the two layers dictates the actuated shapes. Figure 3A shows a strip patterned with elastomer/SMP laminate segments that alternate along the length with a prescribed period to achieve a wavy pattern when heated. Figure 3B shows a similar strip but with patterned segments rotated relative to the long axis of the strip to translate the local bending into macroscopic twist (*32*). The pattern pitch and angle, along with the thickness ratio of the two layers, dictate the geometry (wavelength, diameter, etc.) of the resulting helix. Figure 3C illustrates some of the power of the 3D printing approach to create complex geometries by printing a flat hollow disc that transforms into a wavy disc upon heating. Here, the mechanism driving the wavy pattern is simple bending dictated by the pattern layout, unlike similar structures created with uniform layering but relying on buckling upon heating to create similar wavy disc shapes (*33*–*36*). Also shown for each case are finite element simulations based on the model and measured parameters in Fig. 2A, and they are in good agreement with measurements. This demonstrates an adequate understanding of the phenomena in terms of geometry, material behavior, and process behavior, which can be used broadly to design components with arbitrary shape and complexity.

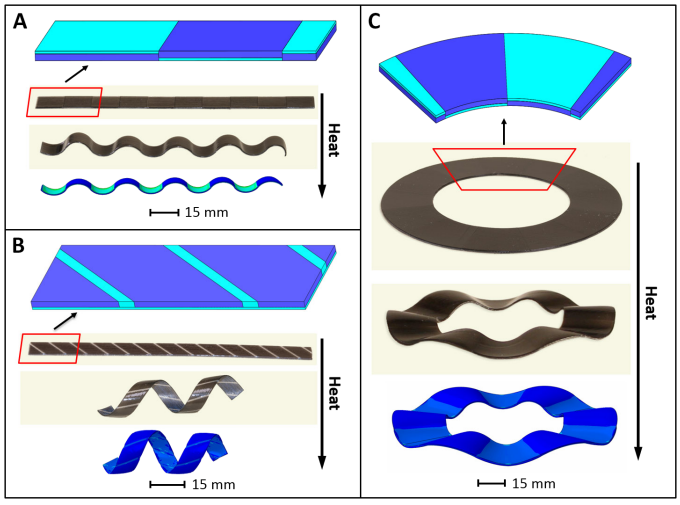

Fig. 3. Direct 4D printing of structural elements with deformation modes dictated by the 3D-printed architecture. (**A**) A printed flat strip (150 mm × 10 mm × 0.7 mm) that transforms into a wavy structure. The SMP/elastomer thicknesses are 0.2/0.5 mm, and the pattern pitch is 15 mm. (**B**) A printed flat strip (120 mm × 8 mm × 0.7 mm) that transforms into a helix. The SMP/elastomer thicknesses are 0.2/0.5 mm, and a 0.5-mm-wide SMP separator is oriented at 45°. (**C**) A ring of 120/68.6-mm outer/inner diameter and 1.2-mm thickness that transforms into a wavy structure. The SMP/elastomer thicknesses are 0.4/0.8 mm, and the pattern pitch is 15 mm. In all cases, the layer printing time is 68 s. Details of the composite architecture are shown in exploded views, where blue represents the elastomer and cyan represents the glassy polymer [see the Supplementary Materials (section S3) for geometry parameters]. Both the temporary (as-printed) and permanent (after heating) configurations from experiments are shown as corresponding finite element simulations.

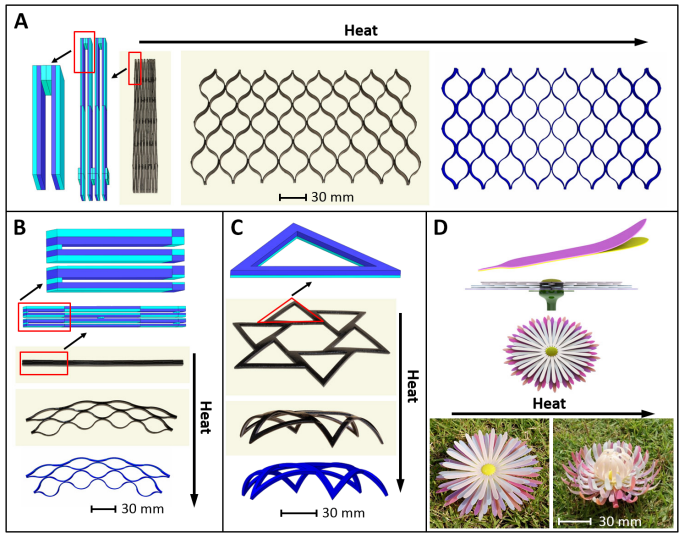

Fig. 4. Direct 4D printing of structures consisting of multiple elements. (**A**) Lattice structure printed in a collapsed configuration (180 mm × 25.2 mm × 7 mm) that deploys into an open configuration upon heating. The SMP/elastomer thicknesses are 0.35/0.35 mm. (**B**) Similar lattice (192 mm × 6.3 mm × 6 mm) structure that not only expands upon heating but also bends because of the designed architecture. The SMP/elastomer thicknesses are 0.8/0.8, 0.6/0.6, 0.3/0.9, and 0.2/0.6 mm, respectively, from top to bottom. (**C**) Flat star-shaped structure that deploys into a 3D dome. Each equilateral triangle has an outer/inner side length of 60/44.4 mm. The SMP/elastomer thicknesses are 0.88/1.77 mm. (**D**) Printed flower consisting of multiple petals at multiple layers that blooms into a configuration, where petals at different layers assume final configurations with different curvatures. The SMP/elastomer thicknesses of all petals are 0.3/0.3 mm. Three different radii (42, 48, and 51 mm) are designed for petals in different layers. Details of the composite architecture are shown in exploded views, where blue represents the elastomer and cyan represents the glassy polymer [see the Supplementary Materials (section S3) for geometry parameters].

Figure 4 demonstrates examples where we apply the concept to structures consisting of many structural elements. Figure 4A shows a lattice architecture that is designed and printed in a compact shape (complete details are given in Materials and Methods and the Supplementary Materials). Upon heating, it markedly deforms with a structural extension of ~900% and a lateral contraction of ~15%. It is notable that, unlike previous examples where the material layering was parallel to the build tray, here, the layering is designed perpendicular to the build tray. Finite element simulations show good agreement, with a predicted extension of 882% and a lateral contraction of 15%. In the Supplementary Materials (fig. S3), we show a similar example, where a structure is printed in an open lattice configuration like in Fig. 4A and then heating collapses it into the compact configuration with a structural compression of ~62%. Figure 4B shows a slight variation of this expanding lattice, where the local layering is now designed to yield a lattice that both expands and bends macroscopically. Figure 4C shows a star-shaped structure that is printed as a flat sheet, and then, each point of the star bends upon heating, raising it out of the plane into a dome. Here, finite element simulations are again in good agreement with measurements. Finally, Fig. 4D shows the design of a complex flower that blooms upon heating. Here, the flower is created so that each petal is a bilayer with the same elastomer-SMP thickness ratio, but the printing time for each layer of petals varies from the bottom to top in a sequence of 25 to 74 s so that, upon heating, each layer of petals curls a different amount, yielding a realistic flower (chrysanthemum) structure. Without changing the geometry of the composite architecture in each layer of petals, we control the curvatures by the management of the printing time only. Of course, one can obtain more freedom in design by varying the macroscopic structure, material architecture, and printing time.

Figure 5 demonstrates the remarkable ability of our 4D-printed structures to be activated into their permanent shape and then to be retrained and stored in multiple temporary shapes. Here, the printed (temporary) shape is a compact lattice (Fig. 4A) that is efficient to print, and the permanent shape after heating is a larger open lattice. We then heated the lattice in its permanent shape (Fig. 5A) to above T_g, where the entire structure is soft, deformed it into a new shape, and cooled to room temperature, where it exhibits significant stiffness. Figure 5 (B to E) shows a number of such programmed shapes, such as saddle-cylinder 3D shape (Fig. 5B), compressed-twisted compact shape (Fig. 5C), semisphere/dome shape (Fig. 5D), and in-plane fan shape (Fig. 5E), which are stable at room temperature until they are deliberately reprogrammed. These are realized by exploiting the shape memory effect of the SMP in these multiple programming operations.

DISCUSSION

We presented a direct 4D printing approach that extends 3D multimaterial photopolymer printing to transform a component from one high-resolution configuration to another with a simple single heating step. This approach opens possibilities in myriad technological applications. One perhaps interesting example is the potential to enable a new product design approach. In essence, the approach is a new manufacturing and assembly process based on the integrated assembly of various parts of a component via programmable compliant mechanisms, that

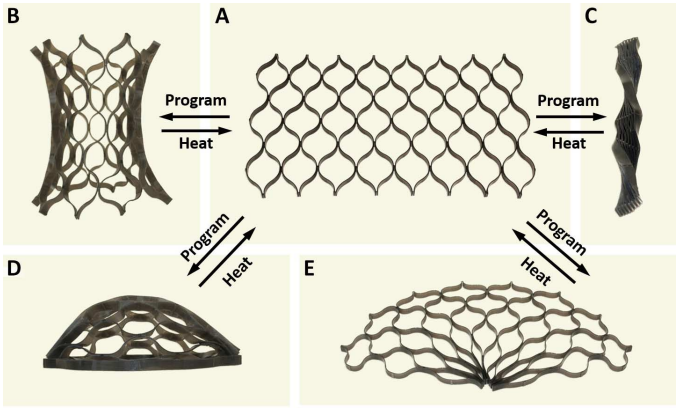

Fig. 5. Demonstration of the ability for a 4D-printed structure to be reprogrammed from its permanent shape into many different configurations that are structurally stiff at room temperature and then to be returned to its permanent shape upon heating. (**A**) The deployed permanent configuration of a compact lattice after heating, which is same with the activated structure in Fig. 4A. This shape is also the recovered shape after reprogramming and heating. (**B**) The reprogrammed saddle-cylinder shape. (**C**) The reprogrammed compressed-twisted compact shape. (**D**) The reprogrammed semisphere/dome shape. (**E**) The reprogrammed in-plane fan shape.

is, design for additive manufacture and compliant assembly. At the outset, we can design geometry, materials, and the fabrication process for two (or more) configurations, rather than a single configuration. A combination of many geometrical, material, and process parameters exists and can be exploited in design. In most of the examples we showed here, we transformed a 2D flat sheet with a purposefully designed material architecture into a 3D structure. The former is easy, fast, and economical to print and requires little or no support material, whereas the latter would, at minimum, be significantly slower, be more expensive, and require significant use of support material. For example, printing the structure of Fig. 4C directly in the 3D dome configuration would require about eight times the time and eight times the support material as compared to the flat 2D configuration when printed on the Objet Connex printer.

In addition, direct 4D printing can serve as a platform technology to integrate functional devices. For example, a flat transformable sheet can be printed. Conductive circuits and electronic devices, such as batteries, sensors, and actuators, can then be assembled on the flat sheet; its flat form makes these integration operations easy. Heating could then deploy the flat structure into a desired 3D structure with built-in electronic functionality. Of course, the heating could be realized by more sophisticated mechanisms, for example, resistive or induction heating that could be localized in both space and time to provide high-fidelity control of the deployment process. Furthermore, one could build the smart flat substrate, with different polymers having different time dependences of their behavior, and achieve a sequenced assembly operation.

Although our approach enables significant opportunities, we would be remiss if we did not mention a drawback. Because the deployment process occurs at an elevated temperature where the structure is soft, it is difficult to deploy the structure when it is in a service situation acted upon by loads, for example, aerodynamic loads in a morphing vehicle scenario. We think that simulation-based composite design concepts that further integrate materials that can tune their stiffness through nonlinear geometrical effects rather than material effects could provide an attractive pathway to this end, and this is the subject of ongoing work.

MATERIALS AND METHODS

Design of samples and 3D printing

All samples were created in the 3D CAD package SolidWorks (Dassault Systèmes). Geometrical descriptions in terms of .stl files were created and imported into the Stratasys Connex Objet multimaterial printer software and printed on Objet500 Connex3, with a slice height of 30 μm under digital printing mode.

Unless stated otherwise, all printed beam-like samples were oriented with the longest side along the x axis (the longest printing distance) of the build tray and the thickness along the z axis. We used the commercial materials TangoBlack+ or Tango+ as the elastomer and VeroClear as the SMP. TangoBlack+ for all samples is represented as blue in the CAD drawings, whereas VeroClear is represented as cyan. Complete geometrical and material details are given in the Supplementary Materials.

Experiments

DMA was carried out on a DMA tester (model Q800, TA Instruments) in tension mode. Samples (~20 mm × 7 mm × 1 mm) for storage modulus and glass transition temperature tests were heated at a ramp rate of 2°C/min and a frequency of 1 Hz. Samples (~25 mm × 8 mm × 0.6 mm) for thermal strain tests were heated/cooled at a ramp rate of 1°C/min under controlled force. Compressive strains in the elastomer or glassy polymer (Fig. 2A) were measured by photographing printed flat strips before and after they were removed from the build tray and then using an image analysis software (ImageJ) to determine the dimension changes at room temperature (~25°C).

Deployment experiments with printed samples were carried out in a Huber CC-118A tank (Peter Huber Kältemaschinenbau) with temperature control, and water was used as the heating medium. Samples were immersed from room temperature into the tank at 62°C. They transformed into their permanent configuration within a few seconds, depending on the specific sample. After ~20 s, the samples had completed the transformation, and we photographed the deformed configuration and subsequently used an image analysis software (ImageJ) to determine the curvature of laminate samples. The samples in Fig. 1D are an exception. These were immersed in the tank, which was at 18°C. The water was then heated at a ramp rate of 2°C/min, the samples were photographed during the heating process, and the curvature was determined via image analysis.

Modeling and simulation

Finite element simulations were conducted to predict the shape change of the printed structures by using the commercially available finite element software package ABAQUS (Dassault Systèmes). For the materials used in the 3D printing, we used the multibranch viscoelastic model to capture its thermoviscoelastic and shape memory behavior; this is briefly described in the Supplementary Materials. The strain that was built into the elastomer during printing was incorporated as a residual thermal strain based on the measured data in Fig. 2A. 2D plane stress models (with CPS4T elements) were built for the printed strips in Fig. 2, whereas 3D models (with C3D8HT elements) were built for the printed structures in Figs. 3 and 4. The geometrical configuration and boundary conditions of the finite element models were the same as those of the samples used in the experiment.

SUPPLEMENTARY MATERIALS

Supplementary material for this article is available at http://advances.sciencemag.org/cgi/content/full/3/4/e1602890/DC1

REFERENCES AND NOTES

1. S. Tibbits, *The Emergence of "4D Printing"* (TED Conferences, 2013).
2. Q. Ge, H. J. Qi, M. L. Dunn, Active materials by four-dimension printing. *Appl. Phys. Lett.* **103**, 131901 (2013).
3. Q. Ge, C. K. Dunn, H. J. Qi, M. L. Dunn, Active origami by 4D printing. *Smart Mater. Struct.* **23**, 094007 (2014).
4. D. Raviv, W. Zhao, C. McKnelly, A. Papadopoulou, A. Kadambi, B. X. Shi, S. Hirsch, D. Dikovsky, M. Zyracki, C. Olguin, R. Raskar, S. Tibbits, Active printed materials for complex self- evolving deformations. *Sci. Rep.* **4**, 7422 (2014).
5. E. J. Pei, 4D printing—Revolution or fad? *Assem. Autom.* **34**, 123–127 (2014).
6. M. P. Chae, D. J. Hunter-Smith, I. De-Silva, S. Tham, R. T. Spychal, W. M. Rozen, Four-dimensional (4D) printing: A new evolution in computed tomography-guided stereolithographic modeling. Principles and application. *J. Reconstr. Microsurg.* **31**, 458–463 (2015).
7. J. Choi, O.-C. Kwon, W. Jo, H. J. Lee, M.-W. Moon, 4D printing technology: A review. *3D Print. Addit. Manuf.* **2**, 159–167 (2015).
8. Q. Zhang, D. Yan, K. Zhang, G. Hu, Pattern transformation of heat-shrinkable polymer by three-dimensional (3D) printing technique. *Sci. Rep.* **5**, 8936 (2015).
9. S. E. Bakarich, R. Gorkin III, M. in het Panhuis, G. M. Spinks, 4D printing with mechanically robust, thermally actuating hydrogels. *Macromol. Rapid Commun.* **36**, 1211–1217 (2015).
10. J. T. Wu, C. Yuan, Z. Ding, M. Isakov, Y. Mao, T. Wang, M. L. Dunn, H. J. Qi, Multi-shape active composites by 3D printing of digital shape memory polymers. *Sci. Rep.* **6**, 24224 (2016).
11. Y. Mao, Z. Ding, C. Yuan, S. Ai, M. Isakov, J. Wu, T. Wang, M. L. Dunn, H. J. Qi, 3D printed reversible shape changing components with stimuli responsive materials. *Sci. Rep.* **6**, 24761 (2016).
12. A. S. Gladman, E. A. Matsumoto, R. G. Nuzzo, L. Mahadevan, J. A. Lewis, Biomimetic 4D printing. *Nat. Mater.* **15**, 413–418 (2016).
13. Q. Zhang, K. Zhang, G. Hu, Smart three-dimensional lightweight structure triggered from a thin composite sheet via 3D printing technique. *Sci. Rep.* **6**, 22431 (2016).
14. Q. Ge, A. H. Sakhaei, H. Lee, C. K. Dunn, N. X. Fang, M. L. Dunn, Multimaterial 4D printing with tailorable shape memory polymers. *Sci. Rep.* **6**, 31110 (2016).
15. Y. Yang, Y. Chen, Y. Wei, Y. Li, 3D printing of shape memory polymer for functional part fabrication. *Int. J. Adv. Manuf. Tech.* **84**, 2079–2095 (2016).
16. M. Zarek, M. Layani, I. Cooperstein, E. Sachyani, D. Cohn, S. Magdassi, 3D printing of shape memory polymers for flexible electronic devices. *Adv. Mater.* **28**, 4449–4454 (2016).
17. S. Hong, D. Sycks, H. F. Chan, S. Lin, G. P. Lopez, F. Guilak, K. W. Leong, X. H. Zhao, 3D printing of highly stretchable and tough hydrogels into complex, cellularized structures. *Adv. Mater.* **27**, 4035–4040 (2015).
18. L. Ionov, Soft microorigami: Self-folding polymer films. *Soft Matter* **7**, 6786–6791 (2011).
19. M. Wehner, R. L. Truby, D. J. Fitzgerald, B. Mosadegh, G. M. Whitesides, J. A. Lewis, R. J. Wood, An integrated design and fabrication strategy for entirely soft, autonomous robots. *Nature* **536**, 451–455 (2016).
20. Y. Osada, A. Matsuda, Shape-memory in hydrogels. *Nature* **376**, 219 (1995).
21. M. Behl, A. Lendlein, Shape-memory polymers. *Mater. Today* **10**, 20–28 (2007).
22. W. M. Huang, Z. Ding, C. C. Wang, J. Wei, Y. Zhao, H. Purnawali, Shape memory materials. *Mater. Today* **13**, 54–61 (2010).
23. H. J. Qi, T. D. Nguyen, F. Castroa, C. M. Yakacki, R. Shandas, Finite deformation thermo-mechanical behavior of thermally induced shape memory polymers. *J. Mech. Phys. Solids* **56**, 1730–1751 (2008).
24. K. Yu, Q. Ge, H. J. Qi, Reduced time as a unified parameter determining fixity and free recovery of shape memory polymers. *Nat. Commun.* **5**, 3066 (2014).
25. Q. Zhao, H. J. Qi, T. Xie, Recent progress in shape memory polymer: New behavior, enabling materials, and mechanistic understanding. *Prog. Polym. Sci.* **49–50**, 79–120 (2015).
26. T. Xie, Tunable polymer multi-shape memory effect. *Nature* **464**, 267–270 (2010).
27. Y. Mao, K. Yu, M. S. Isakov, J. Wu, M. L. Dunn, H. J. Qi, Sequential self-folding structures by 3D printed digital shape memory polymers. *Sci. Rep.* **5**, 13616 (2015).
28. K. Maute, A. Tkachuk, J. Wu, H. J. Qi, Z. Ding, M. L. Dunn, Level set topology optimization of printed active composites. *J. Mech. Des.* **137**, 111402 (2015).
29. L. Huang, R. Jiang, J. Wu, J. Song, H. Bai, B. Li, Q. Zhao, T. Xie, Ultrafast digital printing toward 4D shape changing materials. *Adv. Mater.* **29**, 1605390 (2016)).
30. Z. Zhao, J. Wu, X. Mu, H. Chen, H. J. Qi, D. Fang, Desolvation induced origami of photocurable polymers by digit light processing. *Macromol. Rapid Commun.* **22**, 1600625 (2017).
31. T. Xie, X. Xiao, Self-peeling reversible dry adhesive system. *Chem. Mater.* **20**, 2866–2868 (2008).
32. J. M. Robertson, A. H. Torbati, E. D. Rodriguez, Y. Mao, R. M. Baker, H. J. Qi, P. T. Mather, Mechanically programmed shape change in laminated elastomeric composites. *Soft Matter* **11**, 5754–5764 (2015).
33. Y. Klein, E. Efrati, E. Sharon, Shaping of elastic sheets by prescription of non-Euclidean metrics. *Science* **315**, 1116–1120 (2007).
34. C. D. Santangelo, Buckling thin disks and ribbons with non-Euclidean metrics. *Europhys. Lett.* **86**, 34003 (2009).
35. E. Sharon, E. Efrati, The mechanics of non-Euclidean plates. *Soft Matter* **6**, 5693–5704 (2010).
36. Z. Yan, F. Zhang, J. Wang, F. Liu, X. Guo, K. Nan, Q. Lin, M. Gao, D. Xiao, Y. Shi, Y. Qiu, H. Luan, J. H. Kim, Y. Wang, H. Luo, M. Han, Y. Huang, Y. Zhang, J. A. Rogers, Controlled mechanical buckling for origami-inspired construction of 3D microstructures in advanced materials. *Adv. Funct. Mater.* **26**, 2629–2639 (2016).

Acknowledgments
Funding: We acknowledge the support of an Air Force Office of Scientific Research grant (15RT0885; B.-L. "Les" Lee, program manager). H.J.Q. acknowledges the support of the NSF (CMMI-1462894, CMMI-1462895, and EFRI-1435452). M.L.D. acknowledges support from the SUTD Digital Manufacturing and Design Centre, supported by the Singapore National Research Foundation. **Author contributions:** Z.D. led the experimental efforts with the help of X.P. and C.Y. C.Y. conducted simulations and some experiments. Z.D., T.W., H.J.Q., and M.L.D. contributed to the concept development and manuscript writing. Z.D., C.Y., H.J.Q., and M.L.D. are responsible for all the figures in this paper. All authors reviewed the manuscript. **Competing interests:** M.L.D., Z.D., H.J.Q., and C.Y. filed a patent related to this work: "Active composites with two stable shapes by true 4D printing" (U.S. Patent 62/361,277, 12 July 2016). The other authors declare that they have no competing interests. **Data and materials availability:** All data needed to evaluate the conclusions in the paper are present in the paper and/or the Supplementary Materials. Additional data related to this paper may be requested from the authors.

Submitted 19 November 2016
Accepted 17 February 2017
Published 12 April 2017
10.1126/sciadv.1602890

Citation: Z. Ding, C. Yuan, X. Peng, T. Wang, H. J. Qi, M. L. Dunn, Direct 4D printing via active composite materials. *Sci. Adv.* **3**, e1602890 (2017).